International Journal of Heat and Mass Transfer 78 (2014) 588–598

Contents lists available at ScienceDirect

International Journal of Heat and Mass Transfer

journal homepage: www.elsevier.com/locate/ijhmt

A comparative study of single-/two-jet crossflow heat transfer on a circular cylinder

X.L. Wang [a], J.H. Lee [b], T.J. Lu [a], S.J. Song [b], T. Kim [c,*]

[a] State Key Laboratory for Mechanical Structure Strength and Vibration, Xi'an Jiaotong University, Xi'an 710049, China
[b] School of Mechanical and Aerospace Engineering, Seoul National University, Seoul 151-742, South Korea
[c] School of Mechanical Engineering, University of the Witwatersrand, Wits 2050, Johannesburg, South Africa

ARTICLE INFO

Article history:
Received 16 January 2014
Received in revised form 29 June 2014
Accepted 5 July 2014
Available online 2 August 2014

Keywords:
Circular cylinder
Circumferential heat transfer
Reverse flow region
Two-counter jets
Laminar-to-turbulent transition

ABSTRACT

This study presents thermo-fluidic characteristics on a circular cylinder subject to the impingement of single-/two-counter jets in crossflow. For a fixed circular jet diameter (D_j), the diameter of a target cylinder (D) varies, $D/D_j = 2.5$, 5.0, and 10.0. Two separate scenarios are considered and compared; at a fixed jet Reynolds number, $Re_j = 20{,}000$ and at a fixed total mass flow rate. Results demonstrate that laminar to turbulent transition occurs on a fore cylinder surface which contributes significantly to overall heat transfer. However, it occurs only if the target cylinder is positioned inside the potential core of each jet and only if enough spacing (T) between the jets which is determined by the diameter ratio (D/D_j) as $T = \pi D/2$, is ensured. With small spacing, a reverse flow region formed between the jets ($=\pi D/4$) suppresses the occurrence of the transition. For a fixed jet Reynolds number, the added second jet improves local heat transfer only on the rear cylinder surface whereas the fore cylinder surface is essentially unaffected by the second jet. For a fixed total flow rate, the single impinging jet removes substantially more heat than that achievable by the two-counter jets in the present D/D_j ranges.

© 2014 Elsevier Ltd. All rights reserved.

1. Introduction

Thermo-fluidic characteristics of jets impinging on a flat plate for cooling or heating have long been studied due to its superior heat transfer performance compared to other convective heat transfer schemes. Consequently, a multitude of studies have been conducted [1–4]. It has been established that with a single impinging jet, the overall and local heat transfer on a flat plate depends strongly on many parameters including a jet exit-to-flat plate distance (termed an "impinging distance") [1,3]. The highest heat transfer on a flat plate typically occurs at the stagnation point coinciding with the jet axis at low Reynolds number ranges and low turbulence levels [5,6]. Depending on the impinging distance relative to the potential core of jet flow, either two peaks of local heat transfer (the primary peak at the stagnation point and a second peak off from the stagnation point) or a single peak (only the primary peak at the stagnation point) exist.

In certain applications, the radius of a target surface is finite compared to the infinite radius of a flat plate. The cooling of a circular furnace containing the melt of metal slurry with gaseous pores during the closed-cell foaming process (e.g., via the direct foaming method) [7,8] (Fig. 1) can be an example. In this particular application, many parameters affect the quality of final foam products including those associated with the cooling. A literature survey reveals that previous studies on crossflow multiple jets impinging on a circular cylinder emitting constant heat flux are scares.

Two separate configurations may serve as references to this particular configuration (or application): (i) heat removal from a circular cylinder by an impinging jet and (ii) multiple jets impinging on a flat plate. Some major findings on each reference are separately summarized as follows.

Observations made on circumferential heat transfer characteristics on a circular cylinder (or a convex surface) impinged by single impinging jet [9–17] are: (a) when positioned close to the jet exit (i.e., inside the jet's potential core), a second peak, in addition to a primary peak at the stagnation point, forms; (b) a second peak disappears when positioned relatively far away from the jet exit along the jet axis; (c) flow separation causes a local heat transfer minimum on "small" target cylinders (smaller than the jet diameter) whilst transition from laminar to turbulent flow causes a second peak on "large" target cylinders (larger than the jet diameter), and (d) the overall heat transfer rate decreases as

* Corresponding author. Tel.: +27 11 717 7359.
E-mail address: tong.kim@wits.ac.za (T. Kim).

http://dx.doi.org/10.1016/j.ijheatmasstransfer.2014.07.014
0017-9310/© 2014 Elsevier Ltd. All rights reserved.

Nomenclature

C_f	skin friction coefficient defined in Eq. (10)
C_p	static pressure coefficient defined in Eq. (5)
D	target circular cylinder diameter, m
D_j	circular jet diameter, m
E	voltage from hot-film sensor, V
g	gravitational acceleration, m/s^2
Gr	Grashof number based on cylinder diameter, $Gr = g\beta(T_s - T_j)D^3/\nu^2$
h	convection heat transfer coefficient, W/(m^2 K)
k_f	thermal conductivity of air, W/(m K)
n	the number of jets
Nu	Nusselt number based on a jet diameter defined in Eq. (6)
$p(\alpha)$	static pressure measured at an arbitrary azimuth angle, Pa
p_e	static pressure measured at a jet exit, Pa
q''	heat flux, W/m^2
$\dot{m}$	mass flow rate, kg/s
r	radial coordinate
Re_j	Reynolds number based on a jet diameter defined in Eq. (4)
Ri	Richardson number in Eq. (8)
s	lateral distance from a stagnation point, m
S	cylinder span, m
T	jet-to-jet spacing (=$\pi D/n$), m
T_j	jet temperature measured at a jet exit, K
$T_s(\alpha)$	local temperature measured on a cylinder surface, K
w	axial velocity component of jet flow discharged from a circular jet, m/s
w_e	jet exit velocity at $r = 0$ and $z = 0$, m/s
w_0	centerline (axial) velocity at $r = 0$, m/s
y	coordinate normal to a cylinder surface
z	coordinate coinciding with a jet axis
α	azimuth angle measured from a stagnation point, °
β	thermal expansion coefficient
ρ	density of air, kg/m^3
μ	dynamic viscosity of air, kg/(m s)
ν	kinematic viscosity of air, m^2/s
τ_w	wall shear stress, N/m^2

the impinging distance increases for fixed Reynolds numbers. It has also been reported that a diameter ratio (D/D_j) plays an important role in determining overall heat removal performance: a higher overall heat transfer on a smaller diameter ratio is obtained for a given jet Reynolds number and fixed impinging distance [9–10,14].

For multiple jets impinging on a flat plate, if spacing between neighboring jets and an impinging distance are small, the interference between jets is strong. A region called "a reverse flow region" is formed where counter-flowing streams from the jets meet (on the symmetric axis in Fig. 1). This region lowers the overall rate of heat transfer if the jet flow is confined [18,19] whereas its adverse effect is observed if the jet flow is unconfined [20]. The jet flow leaving the stagnation point formed by each jet experiences initially a favorable pressure gradient but followed by an adverse pressure gradient in a "wall jet region" [21]. With small spacing between the jets, this adverse pressure gradient may be strengthened due to a relatively high pressure existing in the reverse flow region [22]. As a result, laminar to turbulent transition on the flat plate tends to be suppressed.

In the present configuration, jet-to-jet spacing (T) is determined by the number of jets (n) equi-azimuthally distributed over the circumference of a cylinder diameter (D) as $T = \pi D/n$. Since two-counter jets are considered, the two jets are azimuthally positioned at $\alpha = 0°$ and 180° around the cylinder. The following specific issues aim to be addressed.

(i) how jet-to-jet spacing (with two-counter jets, $n = 2$) which is varied with the diameter ratio D/D_j alters local heat transfer characteristics caused by laminar to turbulent transition and a reverse flow region,
(ii) how these two distinctive features are influenced by the relative position to the potential core of the jet flow, and
(iii) for a given total flow rate, a single circular jet or two-counter jets is more effective in terms of overall heat removal from a cylinder.

To this end, the present study experimentally considers two separate configurations: a target cylinder emitting heat which is cooled by (i) a single jet and (ii) two-counter jets for both a fixed jet Reynolds number and a fixed total mass flow rate. The circular jets are positioned at two distinctive impinging distances from a target cylinder – inside/outside the potential core of the jet flow.

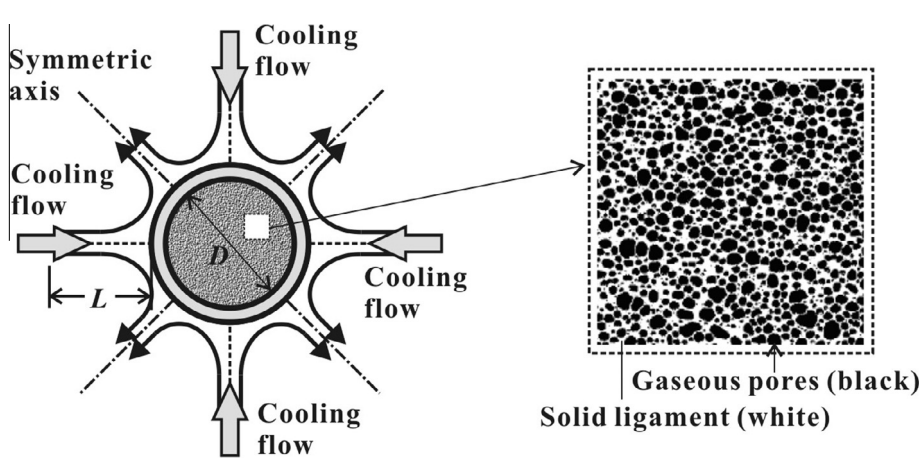

Fig. 1. Schematic of furnace cooling by multiple impinging jets on to a cylindrical furnace containing metal melt with closed-cells.

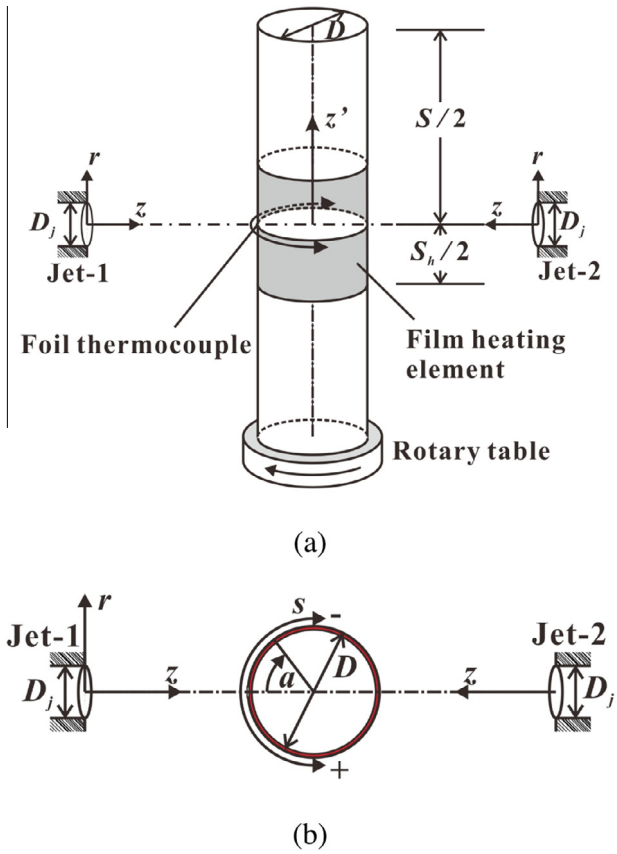

Fig. 2. Schematic of (a) test setup for measuring heat transfer distribution along the circumference of a heated circular cylinder cooled by two-counter jets and (b) crossflow configuration considered.

2. Experimental details

2.1. Test rig and instrumentation

Fig. 2 shows a schematic of the present test rig, consisting of two circular jets, an air supply, and a target cylinder setup for heat transfer measurement. Air at ambient conditions drawn by a centrifugal fan was discharged from circular jets with a fixed diameter of D_j = 26 mm. Each circular jet has an independent settling chamber and a flow control valve. The mass flow rate of each jet was calculated based on the measured flow velocity profile at each jet exit. In addition, a total pressure tapping was inserted at the center of each jet $4D_j$ upstream from the jet exit to ensure that both jets discharge the same mass flow rate. Each circular jet was mounted on a linear traverse system so that the impinging distance could be varied systematically.

To quantify the potential core length of each jet, the jet velocity along the z-axis (centerline jet velocity) was measured using a Pitot tube mounted on an automated linear traverse system. Pressure readings from the Pitot tube were recorded by a differential pressure transducer (DSA™, Scanivalve Inc.). The radial profile of the axial velocity component at selected downstream transverse planes was also measured.

An acrylic circular tube as a target cylinder ($k_s \sim 0.02$ W/m K) was mounted on a rotary table. To obtain circumferential variation of static pressure on the cylinder surface, a static pressure tapping (inner diameter of 0.5 mm) was drilled into the cylinder surface and rotated with a 2.5° increment to cover the full circumferential range from $\alpha = 0°$ (a stagnation point) to $\alpha = 360°$.

Table 1
Parameters of test setup and conditions.

Test parameter	Value
Circular jet diameter, D_j	0.026 m
Circular cylinder diameter, D	0.065 m, 0.13 m, 0.26 m
Relative curvature, D/D_j	2.5, 5.0, 10.0
Total mass flow rate, $\dot{m}$	0.017 kg/s
Reynolds number, Re_j	Single jet: 20,000; 40,000 Two-counter jets: 20,000
Circular cylinder span, S	0.48 m
Width of heating element, S_h	0.20 m
Constant heat flux, q''	2500 W/m^2

For heat transfer measurement, a film-type heating element with a thickness of 0.32 mm that simulates constant heat flux was attached to the outer surface of a target cylindrical Perspex tube having its outer diameter of D (listed in Table 1). The thickness of the tube was 5 mm and the target cylinder was filled with a low thermal conductivity foam as a thermal insulation to minimize heat loss. The net heat flux, q'' was estimated as,

$$q'' = q''_{input} - q''_{cond} - q''_{rad} \tag{1}$$

where q''_{input} is the input heat flux from the film heater calculated based on the input current (I) and voltage (V) from a DC power supply to the heater ($q''_{input} = IV$), and q''_{cond} and q''_{rad} are respectively heat losses via conduction and radiation. The conductive heat loss occurring through the target cylinder's thickness was estimated using Fourier's law. The radiative heat loss was calculated by Stefan–Boltzmann's law as,

$$q''_{rad} = \varepsilon\sigma(T_s^4 - T_a^4) \tag{2}$$

where ε is the emissivity, σ is the Stefan–Boltzmann constant, T_s is the cylinder surface temperature, and T_a is the ambient temperature. The emissivity (ε) was obtained by adjusting the emissivity setup in an infrared (IR) camera to match the cylinder temperature readings from flush mounted film-type thermocouples and estimated to be $\varepsilon = 0.98$.

Azimuthal location of laminar to turbulent transition on a target cylinder may be indicated by wall shear stresses. To this end, a hot-film sensor (55R47 Dantec Inc.) with a thickness of 50 μm was flush mounted on the cylinder surface. The wall shear stress was calculated from the electrical voltage of the hot-film sensor using King's law as [23–25]:

$$\tau_w^{1/3} = AE^2 + B \tag{3}$$

where E is the voltage from the hot-film sensor, A and B are the constants determined from the present hot-film sensor calibration using a hot-wire anemometry, following a method suggested by Desgeorges et al. [26]. To calibrate the hot-film sensor, the circular cylinder was immersed in uniform flow in a blow-down wind-tunnel and was set to a certain azimuth angle whilst the free-stream velocity was varied. At each flow velocity, E and τ_w were calculated based on the velocity profile normal to the cylinder surface at this azimuth angle, by the hot-wire anemometry. τ_w and E were then correlated to obtain the constants A and B.

2.2. Data reduction parameters and measurement uncertainties

The jet Reynolds number is defined based on the jet diameter D_j and centerline jet velocity w_e measured at the jet exit, as:

$$\mathrm{Re}_j = \frac{\rho w_e D_j}{\mu} \tag{4}$$

The local static pressure distribution was evaluated using the dimensionless pressure coefficient defined as:

$$C_p(\alpha) = \frac{p(\alpha) - p_e}{\rho w_e^2/2} \tag{5}$$

where $p(\alpha)$ is the static pressure measured on the cylinder surface at an arbitrary azimuthal location and p_e is the static pressure measured at the jet exit.

The heat transfer characteristics were evaluated using the Nusselt number defined based on the jet diameter D_j as,

$$Nu(\alpha) = \frac{h(\alpha)}{k_f/D_j} \tag{6}$$

where

$$h(\alpha) = \frac{q''}{T_s(\alpha) - T_j} \tag{7}$$

Here, q'' is the estimated net heat flux (Eq. (1)), k_f is the thermal conductivity of air whilst T_s and T_j are the local surface temperature and jet flow temperature at the jet exit $z = 0$, respectively. The origin of the azimuth angle α coincides with the geometric stagnation point.

In mixed convection problems where natural convection and forced convection co-exist, Richardson number ($Ri = Gr/Re_j^2$) represents that which mode dominates between natural and forced convection and is defined as,

$$Ri = \frac{g\beta(T_s - T_j)D}{w_e^2} \tag{8}$$

where g is the gravitational acceleration, β is the thermal expansion coefficient, T_s is the wall temperature, T_j is the jet temperature, D is the cylinder diameter, and w_e is the jet exit velocity. Typically, the natural convection is negligible when $Ri < 0.1$, forced convection is negligible when $Ri > 10$, and neither is negligible when $0.1 < Ri < 10$. In the present study, with the highest wall temperature ($T_s = 90$ °C) at the rear side of the largest cylinder ($D = 260$ mm), the local Richardson number is calculated to be,

$$Ri = \frac{g\beta(T_s - T_j)D}{w_e^2} = \frac{9.8 \times 3.33 \times 10^{-3} \times (90 - 20) \times 0.26}{14^2} = 3.0 \times 10^{-3} \ll 0.1 \tag{9}$$

Thus, the natural convection effect is neglected.

The skin friction coefficient is defined as:

$$C_f = \frac{\tau_w}{\rho w_e^2/2} \tag{10}$$

where τ_w is the wall shear stress defined as

$$\tau_w = \mu \frac{\partial u}{\partial y} \tag{11}$$

Here, y is the direction normal to the cylinder surface, u is the velocity component parallel to the cylinder surface, μ is the dynamic viscosity of air, and ρ is the density of air.

The uncertainty associated with the azimuth angle was found to be within ±0.2°. The measurement uncertainty of the Reynolds number and the static pressure coefficient was estimated using a method reported in reference [27] (based on 20:1 odds) and found to be within 1.3% and 2.8%, respectively. The resolution of the temperature readings from the temperature scanner was ±0.1 K for each thermocouple. With the heat losses of approximately 1% (conduction) and 12% (radiation) accounted for, the uncertainty of the Nusselt number was calculated to be within 5.1%. The uncertainty associated with the hot-wire measurement was estimated to be within 0.8%, resulting in 4.44% of the uncertainty in C_f.

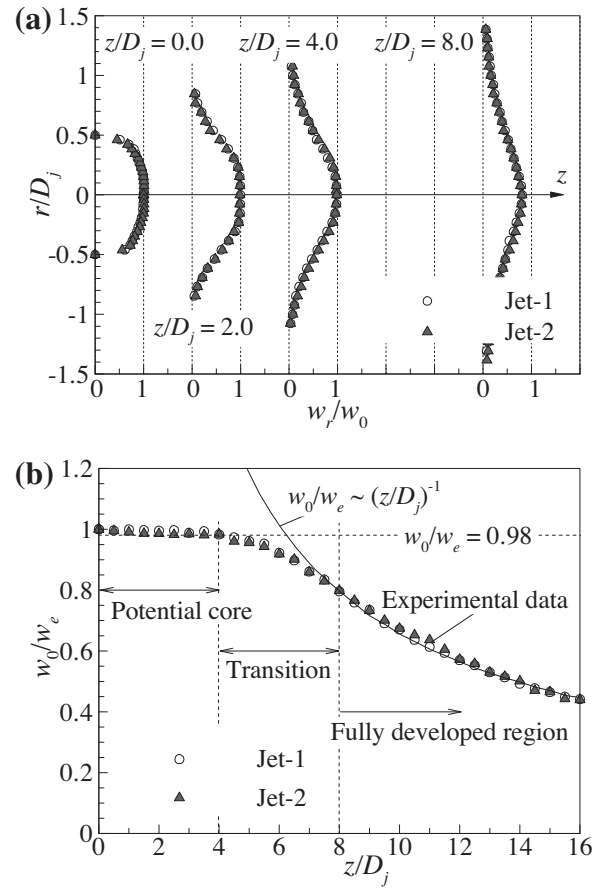

Fig. 3. Free jet characteristics of the two jets at $Re_j = 20{,}000$: (a) the radial profile of axial velocity at selected downstream transverse planes; (b) the axial variation of normalized centerline velocity, indicating a potential core persisting up to $z/D_j = 4.0$.

3. Discussion of results

3.1. Circular jet characteristics in free exit

The potential core length and the velocity profiles indicate jet characteristics that influence local and overall heat transfer on a target cylinder. Fig. 3(a) exhibits the radial profiles of the axial velocity component at selected traverse planes and indicates a symmetric flow field with respect to the jet axis. According to the classical description of free jet flow structures [28], there exist three distinctive flow regions: (a) the initial region, (b) the transitional region, and (c) the fully developed region. In the initial region, the jet velocity along the jet axis maintains its magnitude as high as that at the jet exit. There exists a region where the jet flow is undisturbed by the flow interaction with the surrounding fluid at rest (submerged jet), the so-called "potential core." For turbulent circular jets, Martin [1] suggested that the core length persists up to $4D_j$ whilst Gautner [4] reported that it typically ranges from $4.7D_j - 7.7D_j$. After the jet flow is fully developed via transition, the axial velocity profiles become self-similar, collapsing onto a single curve that could be fitted using Gaussian distribution [29].

The potential core length of the present circular jets in the free exit was quantified by traversing the centerline jet velocity w_0 at $r = 0$ and the results are plotted in Fig. 3(b) where the centerline velocity w_0 is normalized by that measured at the jet exit, w_e. Following the definition of Giralt et al. [30] that the potential core length is the distance from a nozzle exit to an axial point where the centerline velocity w_0 is 98% of the jet exit velocity w_e, it is derived from Fig. 3(b) that both free jets have the potential core

length, $z/D_j = 4.0$. Inside the potential core ($z \leqslant 4.0D_j$), the centerline velocity has the same magnitude as w_e. Outside the potential core (i.e., $z > 4.0D_j$), the axial centerline velocity w_0 decays inversely proportional to the axial distance [28], as:

$$\frac{w_0}{w_e} \sim \left(\frac{z}{D_j}\right)^{-1} \tag{12}$$

The measured centerline velocity data followed the trend expressed by Eq. (12) after $z/D_j = 8.0$. According to Abramovich [28], the onset of the fully developed region (or self-similar region) occurs approximately at $z/D_j = 8.0$.

It should be noted that the characteristics of the present two jets in the free exit are expected to vary due to the presence of a cylinder downstream, but assumed to be consistent amongst the three selected diameter ratios. Hofmann et al. [6] argued that the jet flow structure affected by the presence of a flat plate is limited within approximately $1.0D_j$ upstream from the flat plate. Similarly, only within $1.0D_j$ upstream from a convex surface, the flow structure was found to be affected [31]. Hence, other flow regions away from the target surface are expected to remain unaffected.

3.2. Crossflow consideration

Before proceeding further, it is instructive to provide the credibility of the present experimental setup. To this end, lateral heat transfer distributions on a flat plate positioned at $z/D_j = 4.0$ and 6.0 are compared to the data reported in Refs. [32,33]. Good agreement is obtained in Fig. 4 except a slight deviation in the stagnation region, which may be caused by different turbulence levels at the jet exit [5].

Present study only considers heat transfer characteristics in a single plane as illustrated in Fig. 2(b) (i.e., a crossflow plane) although the flow discharged from circular jets interacting with a target cylinder is three-dimensional. Unlike a circular jet impinging on a flat plate whose thermal flow field is axisymmetric, the crossflow consideration simplifies the actual three-dimensional problem.

The overall temperature contours on the three selected cylinders are shown in Fig. 5, captured by a pre-calibrated infrared (IR) camera. The impinging distance was set to be $z/D_j = 8.0$ at $Re_j = 20{,}000$. Isothermal lines on the cylinder ($D/D_j = 2.5$) form an ellipse-like shape; slightly wider in the z'-direction (coinciding with the target cylinder's axis) than in the s-direction (along the circumference). On bigger cylinders ($D/D_j = 5.0$ and 10.0), isothermal lines turn to a circular shape.

To quantify this, the temperature data was extracted along the two selected directions and the results are plotted in Fig. 6. On the

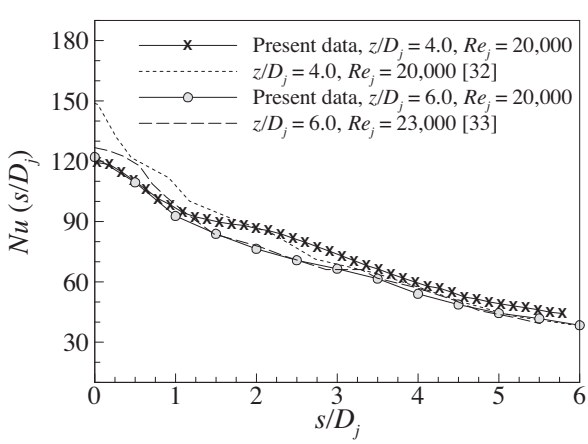

Fig. 4. Comparison of lateral heat transfer distributions on a flat plate subject to a normal impinging jet to the data reported by Lee et al. [32] and Goldstein and Franchett [33].

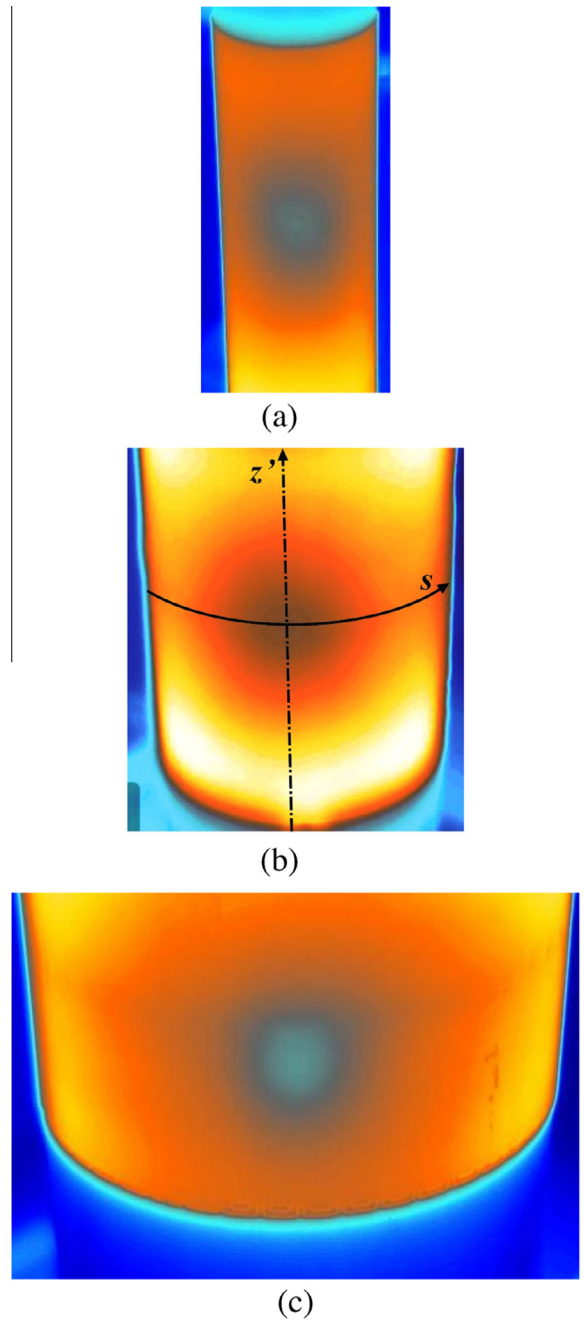

Fig. 5. Temperature contours on a circular cylinder subject to a circular impinging jet at $z/D_j = 8.0$ (outside the potential core) captured by an infrared (IR) camera; (a) $D/D_j = 2.5$; (b) $D/D_j = 5.0$; (c) $D/D_j = 10.0$.

cylinders, the temperature distribution, at least, along these two selected directions is almost identical whereas there is a deviation on the smaller cylinder surface ($D/D_j = 2.5$) where a slightly steeper temperature drop exists along the circumference (the s-direction) than that along the z'-direction. The crossflow consideration simplifies the three-dimensional heat transfer analysis but may provide useful information on the present problem.

3.3. Heat transfer on a small cylinder ($D/D_j = 2.5$)

Local heat transfer characteristics on a cylinder of $D/D_j = 2.5$ subject to the impingement of both a single jet and two-counter jets in crossflow are considered at the jet Reynolds number of $Re_j = 20{,}000$. Detailed circumferential distribution of heat transfer,

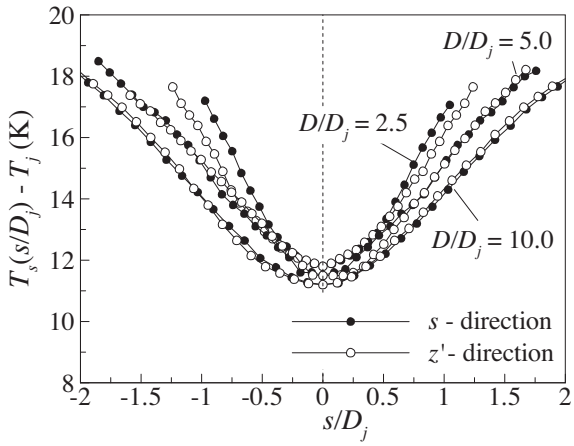

Fig. 6. Comparison of temperature distribution along the *s*-direction and the *z'*-direction for three selected cylinders subject to a single circular impinging jet at $Re_j = 20{,}000$.

static pressure, and skin friction is measured at two distinctive impinging distances; $z/D_j = 2.0$ (inside the potential core) and $z/D_j = 8.0$ (outside the potential core).

3.3.1. Circumferential heat transfer distribution with a single impinging jet

At $z/D_j = 2.0$ (inside the potential core), the local heat transfer on the cylinder surface decreases from the stagnation point $\alpha = 0°$ where the maximum heat transfer exists, and reaches a local minimum at $\alpha = 50°$ (Fig. 7(a)). Afterwards, the local heat transfer turns to increase slightly until forming a peak at $\alpha = 80°$ (termed a "second peak" in addition to the primary peak at $\alpha = 0°$). It then decreases monotonically to $\alpha = 180°$.

Two possible causes for the observed local minimum and subsequent second peak are flow separation and/or laminar to turbulent transition. Static pressure distribution along the cylinder surface can indicate flow separation, if responsible, where a local minimum of heat transfer typically coincides with the inflection point on static pressure curves. Results in Fig. 7(b) exhibit that the static pressure peaks at $\alpha = 0^o$ and decreases until $\alpha = 40°$, followed by a gradual increase to $\alpha = 180°$. It can be concluded that flow separation plays no part in the formation of the second peak.

The distribution of skin friction along the cylinder surface is now considered to examine whether laminar to turbulent transition is responsible for the second peak. Results in Fig. 7(c) show that the maximum skin friction (C_f) exists approximately at $\alpha = 25°$. After attaining its maximum value, the skin friction falls rapidly to a certain value at around $\alpha = 50°$. After which, it forms a plateau region up to $\alpha = 80°$, followed by a monotonic decrease to zero skin friction. By comparing the azimuthal distribution of the heat transfer and skin friction coefficients, it may be inferred that the onset of the transition occurs at the azimuthal location where the plateau region of the skin friction begins to form (Fig. 7(c)) and the observed second peak takes place at the azimuth angle where the skin friction starts to drop from the plateau region.

At $z/D_j = 8.0$ (outside the potential core), the local heat transfer decreases monotonically from the stagnation point $\alpha = 0°$ to the rear side of the cylinder at $\alpha = 180°$ (Fig. 7(a)). The local heat transfer at the stagnation point is marginally higher than that of the cylinder positioned inside the potential core. Locally, a second peak is not formed. The disappearance of the second peak has been argued by Jambunathan et al. [3] as follows. A series of toroidal vortices that form in the shear region around the circumference of the jet are convected downstream. Subsequently these vortices merge into large vortices and brake down into small-scale random

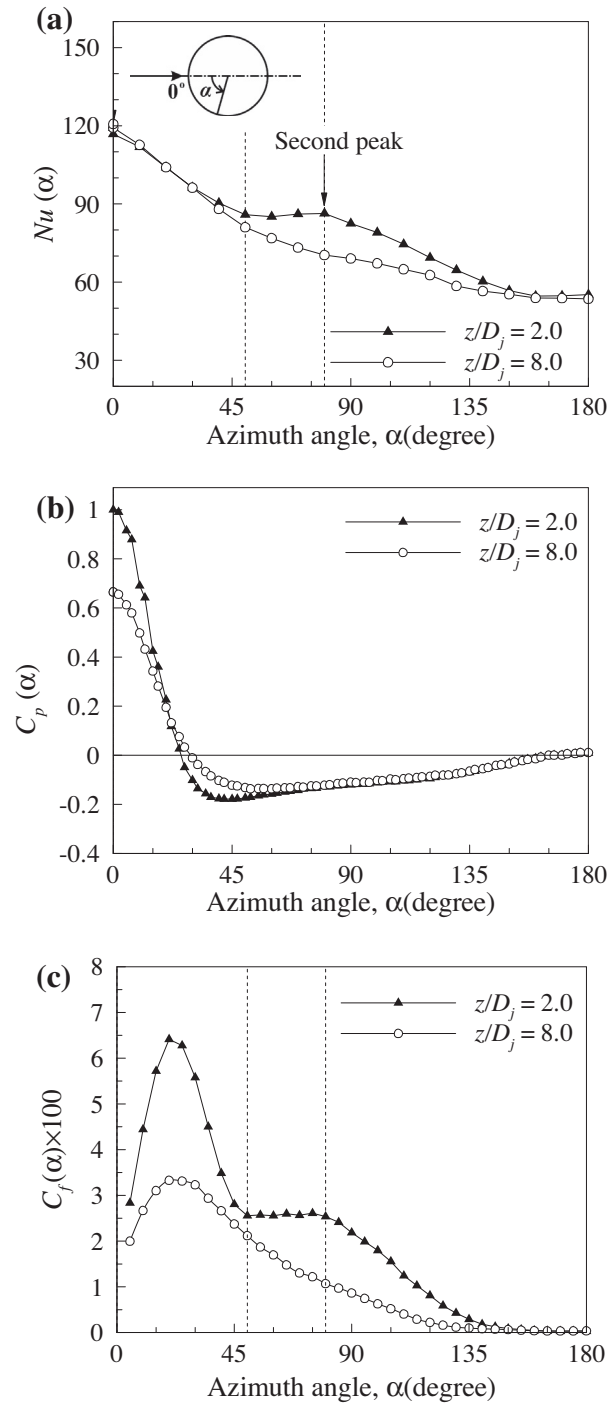

Fig. 7. Circumferential distributions of (a) Nusselt number (*Nu*), (b) static pressure coefficient (C_p), and (c) skin friction coefficient (C_f) on a target cylinder ($D/D_j = 2.5$) subject to a single impinging jet at $Re_j = 20{,}000$.

turbulence that penetrates into the jet axis. This penetration causes the radial (or lateral) oscillation of flow on the flat plate, resulting in the break-down of any distinct flow features including flow transition from laminar to turbulent flow. This argument appears to hold for the present impinging jet on a cylinder surface at $z/D_j = 8.0$.

3.4. Comparison at a fixed jet Reynolds number

Impinging jet heat transfer with a single jet and two-counter jets in crossflow is compared for a fixed jet Reynolds number,

Re_j = 20,000. The total mass flow rate discharged from the two-counter jets is doubled. Two additional cylinders D/D_j = 5.0 and 10.0 are also considered under the same test conditions. Each target cylinder is positioned in two distinctive positions; z/D_j = 2.0 (inside the potential core) and 8.0 (outside the potential core).

3.4.1. Inside the potential core

On the small cylinder (D/D_j = 2.5) subject to a single jet, the local heat transfer at the stagnation point (α = 0°) is the highest as shown in Fig. 8(a). After which, the local heat transfer is decreased until the laminar to turbulent transition elevates the local heat transfer, followed by a second peak formed at α = 80°.

With two-counter jets, two primary peaks exist at α = 0° and 180°. Since the jet Reynolds number was fixed for both jets, the primary peaks have identical magnitude. At α = 90° the reverse flow region is formed where the fluid streams from the two counter-jets meet and are deflected away from the cylinder surface. It is interesting to notice that the local heat transfer on the fore cylinder region for each jet is unaffected by the other jet, separated virtually by the reverse flow region.

On the bigger cylinders e.g., D/D_j = 5.0 and 10.0 (Fig. 8(b) and (c)), the relative azimuthal range under the influence of the laminar to turbulent transition by the single jet becomes narrower. With the two-counter jets, the enhanced local heat transfer in the reverse flow region diminishes. However, another second peak emerges. On these larger cylinders, the flow that follows the cylinder surface after its stagnation has enough spacing for the laminar to turbulent transition to occur before reaching the reverse flow region where a higher pressure exists. Also, similarly, the local heat transfer on the fore cylinder region for each jet is unaffected by the second jet, separated virtually by the reverse flow region.

In both cases: single jet/two-counter jets, the azimuthal location of the second peak (due to the transition) varies with the D/D_j ratio. However, it has been argued that on a flat plate subject to a circular impinging jet, laminar to turbulent transition causes a second peak consistently at $2.0D_j$ measured from the stagnation point, preceded by a local minimum roughly at $1.5D_j$ [3]. To facilitate the comparison, the data in Fig. 9 were re-plotted in Fig. 9 as a function of a lateral distance (s/D_j) instead of the azimuth angle (α) where s is the absolute lateral distance measured from the stagnation point.

The present onset location of laminar to turbulent transition is s/D_j = 1.5 regardless of the D/D_j ratio, followed by the formation of the second peak roughly at s/D_j = 2.0. This lateral location of the second peak is consistent with that expected on a flat plate that is positioned inside the potential core.

In summary, the addition of a second jet positioned at α = 180° strengthens the local heat transfer on the rear side of the cylinder (i.e., from α = 180° to α = 90°). However, the other side of the cylinder (i.e., from α = 0° to α = 90°) is essentially unaffected. In other words, each jet determines local heat transfer in the fore half of the cylinder with respect to the symmetric axis at α = 90°. The two-counter jets enhance only about 17.0% for D/D_j = 2.5, 38% for

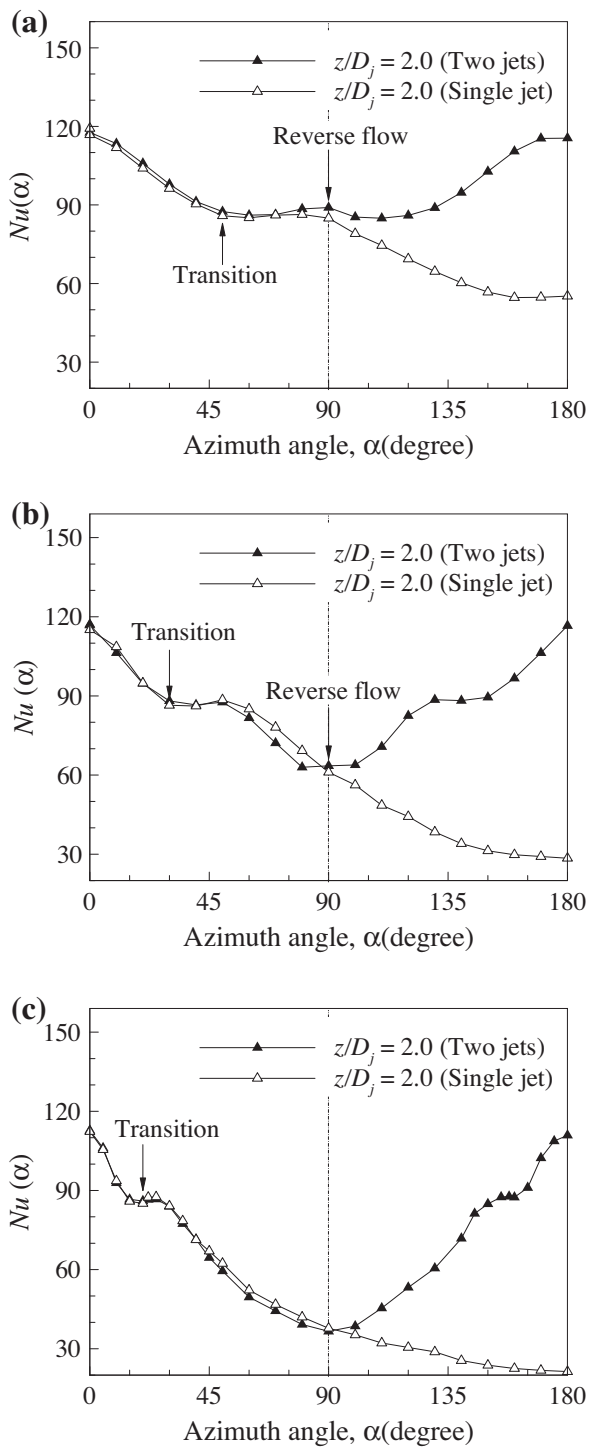

Fig. 8. Comparisons of local Nusselt number distribution on three selected cylinders positioned at z/D_j = 2.0 (in potential core region) subject to a single and two-counter impinging jets for a fixed jet Reynolds number of 20,000; (a) D/D_j = 2.5; (b) D/D_j = 5.0; (c) D/D_j = 10.0.

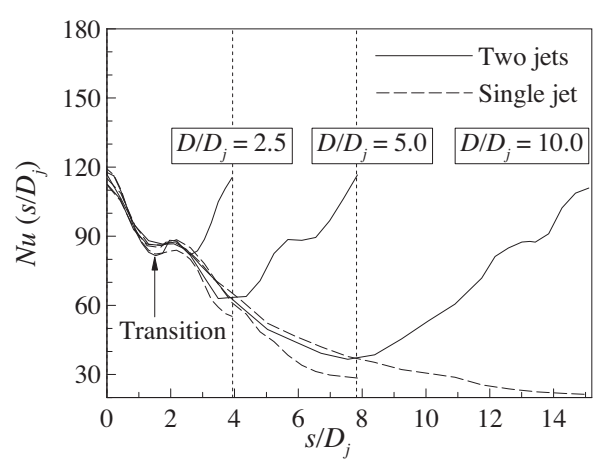

Fig. 9. Lateral distribution of local Nusselt number on three selected cylinders positioned at z/D_j = 2.0 subject to a single and two-counter impinging jets for a fixed jet Reynolds number of 20,000.

D/D_j = 5.0, and 43% for D/D_j = 10.0 higher overall heat transfer than the single jet even with the doubled total mass flow rate.

3.4.2. Outside the potential core

At z/D_j = 8.0, the local heat transfer with the single jet is monotonically decreased from the stagnation point without forming a second peak regardless of the D/D_j ratio (Fig. 10). With the two-counter jets, a second peak is formed resulting not from laminar to turbulent transition but from the formed reverse flow region at $\alpha = 90°$. However, the elevated local heat transfer in this region diminishes as the target cylinder becomes bigger. About 23% more for D/D_j = 2.5, 35% more for D/D_j = 5.0, and 34% more for D/D_j = 10.0 of the overall heat transfer enhancement are achievable with the two-counter jets although the total mass flow rate was doubled. The addition of a second jet positioned at $\alpha = 180°$ strengthens the local heat transfer only on the rear side of the cylinder (i.e., from $\alpha = 180°$ to $\alpha = 90°$). The other side of the cylinder (i.e., from $\alpha = 0°$ to $\alpha = 90°$) is essentially unaffected.

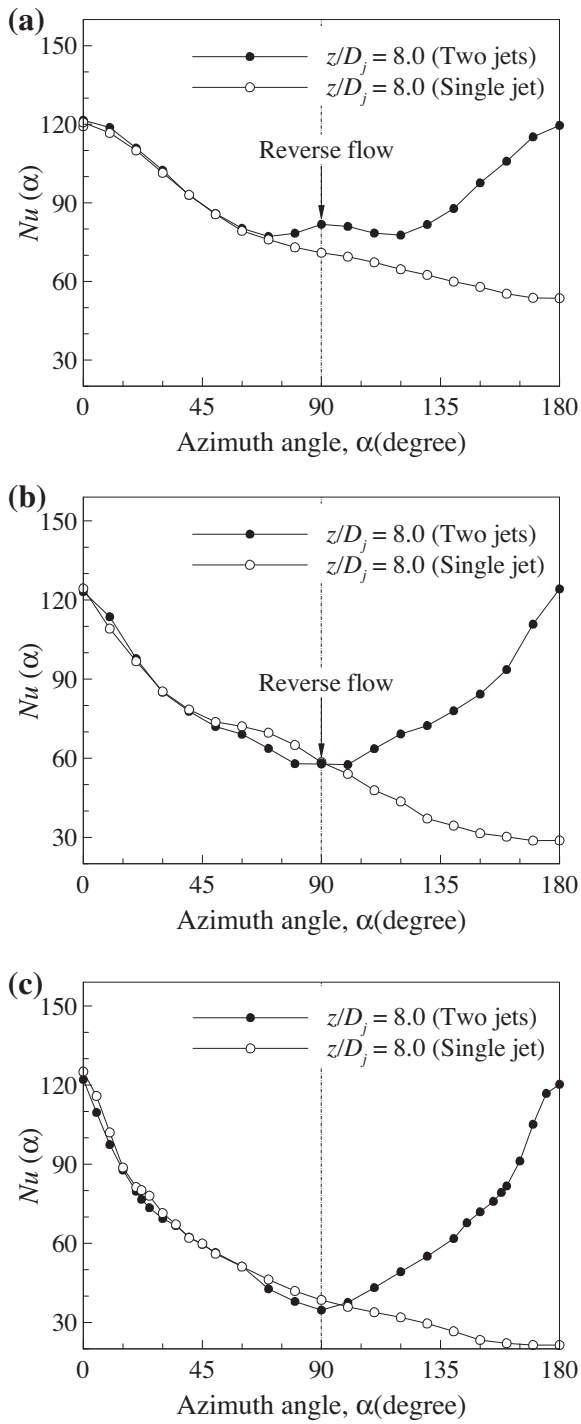

Fig. 10. Comparisons of local Nusselt number distribution on three selected cylinders positioned at z/D_j = 8.0 (in fully developed flow region) subject to a single and two-counter impinging jets for a fixed jet Reynolds number of 20,000; (a) D/D_j = 2.5; (b) D/D_j = 5.0; (c) D/D_j = 10.0.

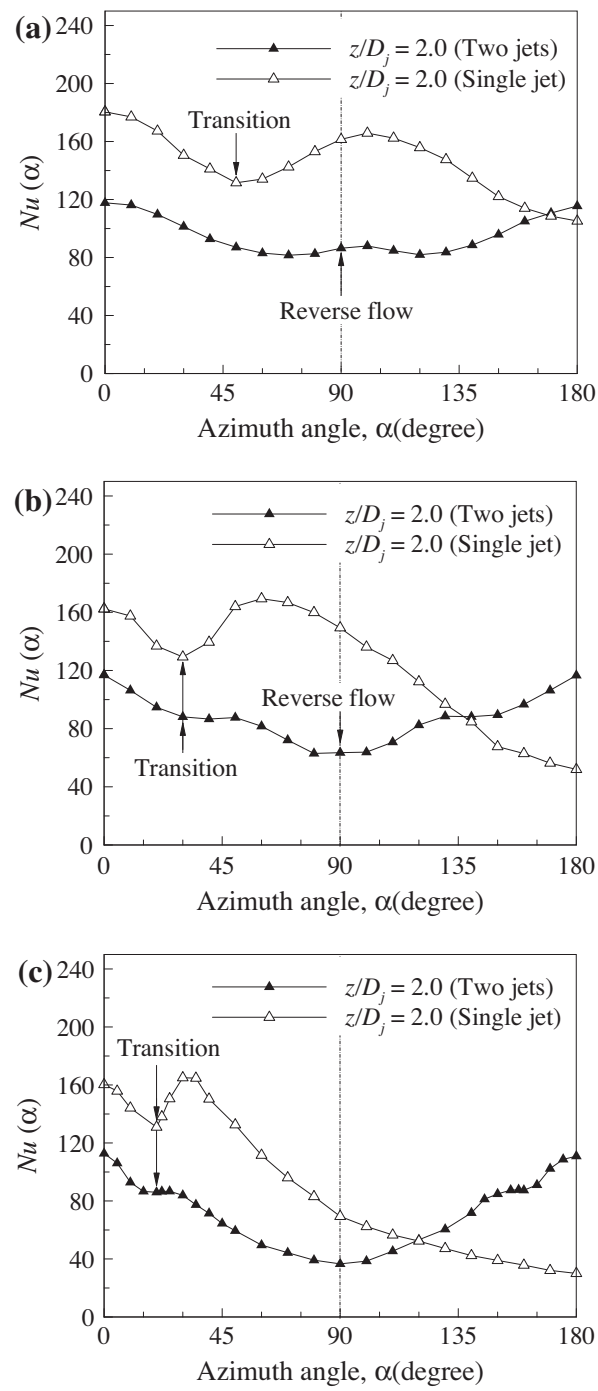

Fig. 11. Comparisons of local Nusselt number distribution on three selected cylinders positioned at z/D_j = 2.0 (in potential core region) subject to a single and two-counter impinging jets for a fixed total mass flow rate; (a) D/D_j = 2.5; (b) D/D_j = 5.0; (c) D/D_j = 10.0.

3.5. Comparison at a fixed total mass flow rate

It is practically more relevant that the total mass flow rate discharged both from the two-counter jets and from the single jet is fixed i.e., $Re_j = 20{,}000$ (for the two-counter jets) and $Re_j = 40{,}000$ (for the single jet) for comparison. Detailed local heat transfer distribution on a cylinder cooled by the single jet and two-counter jets is discussed separately.

3.5.1. Inside the potential core

Fig. 11(a) shows that on $D/D_j = 2.5$, the single jet causes the highest heat transfer at the stagnation point and the local heat transfer is increased by the laminar to turbulent transition from $\alpha = 50°$, forming a second peak at $\alpha = 100°$. The transition elevates the local heat transfer substantially leading to its magnitude as high as that of the stagnation point. The circumferential region under the influence of the transition covers more than half of the total cylinder surface. Considering the two jets with each jet discharging half of the fixed total mass flow rate, heat removed at each stagnation point is about 70% of that removable by the single jet that has the doubled jet Reynolds number. The single jet provides 53% higher overall cooling performance than that achievable by the two-counter jets.

On larger cylinders $D/D_j = 5.0$ and 10.0 (Fig. 11(b,c)), the higher heat transfer regions induced by the transition are formed but their relative azimuthal range becomes narrower. However, the contribution of the reverse flow region to the overall heat transfer becomes minimal. The local heat transfer on the rear side of the cylinder with the single jet drops significantly. Still, the single jet is able to remove more heat than the two-counter jets (40% more for $D/D_j = 5.0$ and 22% more for $D/D_j = 10.0$).

To examine the absolute onset location of the transition for all the considered cases, the data plotted in Fig. 11 is re-plotted in Fig. 12. The transition starts at $s/D_j = 1.5$ and the second peak forms at $s/D_j = 2.0$. It may be concluded that the onset location of the laminar to turbulent transition is solely determined by the jet diameter which is consistent with an impinging jet on a flat plate. The target cylinder size and jet Reynolds number play no part in determining the onset location if the transition occurs.

3.5.2. Outside the potential core

At $z/D_j = 8.0$, the single jet having the doubled jet Reynolds number causes a monotonic decrease in local heat transfer from the stagnation point without forming a second peak (Fig. 13). Similar to the cylinder positioned in the potential core, the magnitude of the local heat transfer by the single jet in most of azimuthal ranges is higher than that with the two-counter jets. On larger cylinders, the local heat transfer enhancement due to the reverse flow region diminishes.

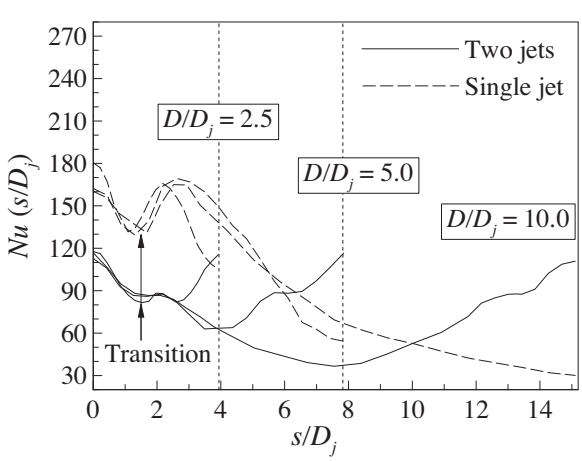

Fig. 12. Lateral distribution of local Nusselt number on three selected cylinders positioned at $z/D_j = 2.0$ subject to a single and two-counter impinging jets for a fixed total mass flow rate.

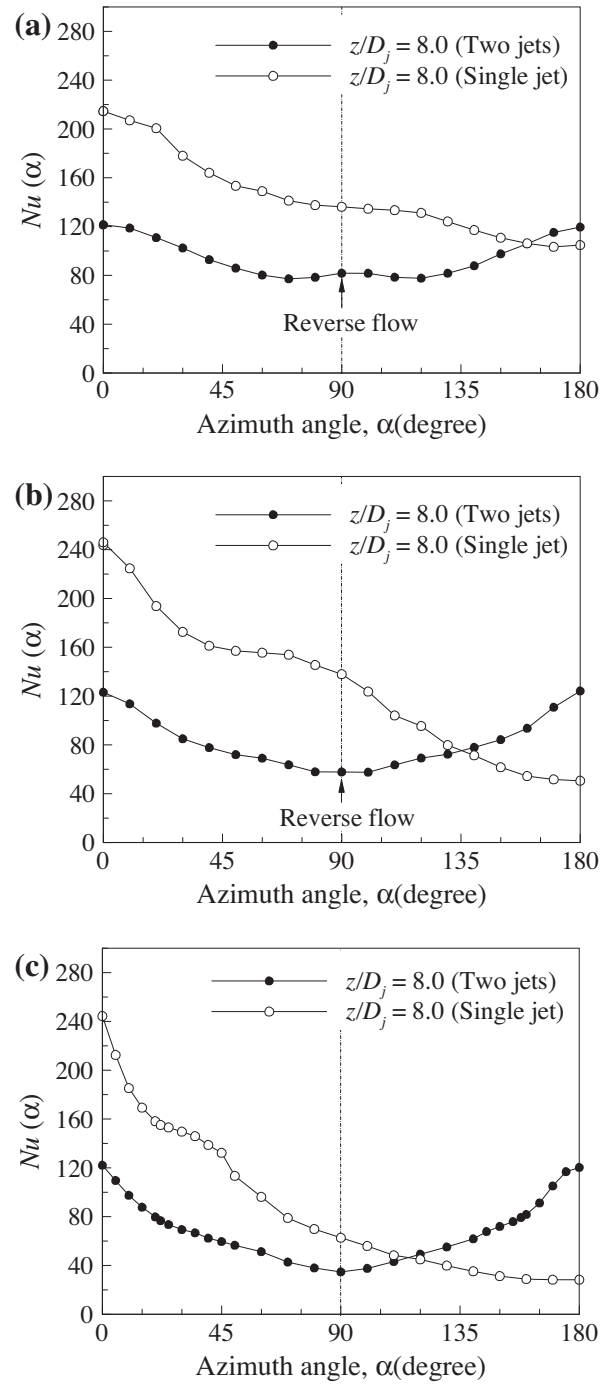

Fig. 13. Comparisons of local Nusselt number distribution on three selected cylinders positioned at $z/D_j = 8.0$ (in fully developed flow region) subject to a single and two-counter impinging jets for a fixed total mass flow rate; (a) $D/D_j = 2.5$; (b) $D/D_j = 5.0$; (c) $D/D_j = 10.0$.

3.5.3. Summary

For a fixed total mass flow rate, the single jet removes more heat than the two-counter jets, which is counter-intuitive. Even with the cylinder being 10 times as large as the circular jet i.e., $D/D_j = 10.0$, the single jet provides the superior cooling capacity.

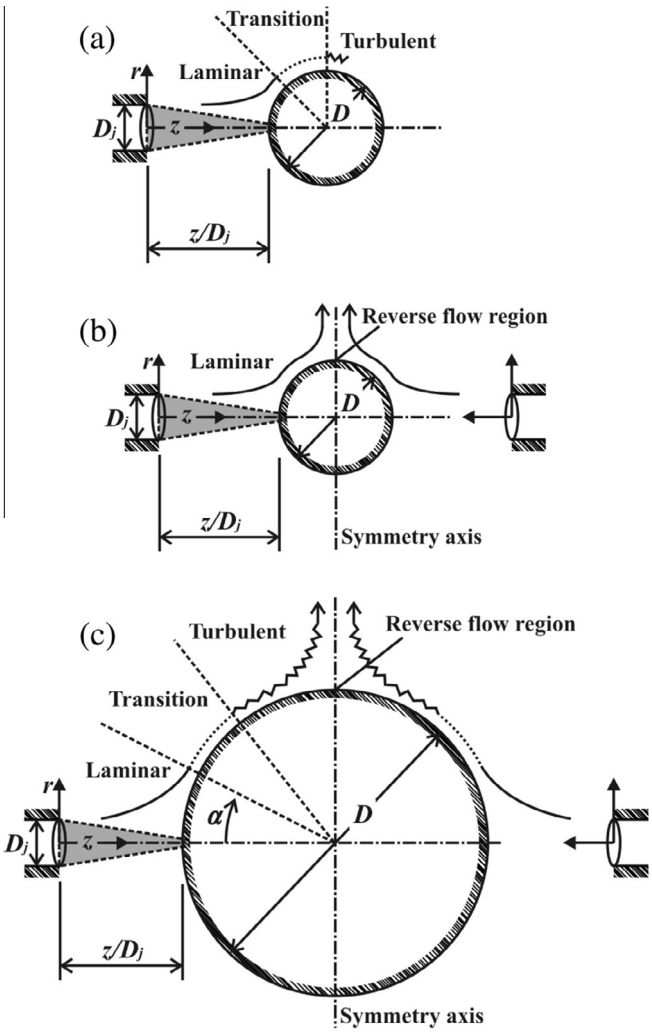

Fig. 14. Sketches of flow regions on a single cylinder subject to single / two-counter jets positioned in potential core region; (*a*,*b*) $D/D_j = 2.5$; (c) $D/D_j = 5.0$ and 10.0.

This is due to the fact that the enhanced rear side local heat transfer by the added second counter jet does not contribute to the overall heat transfer significantly. It is more effective to concentrate the cooling flow on the fore cylinder region which determines the overall heat transfer of the target cylinder.

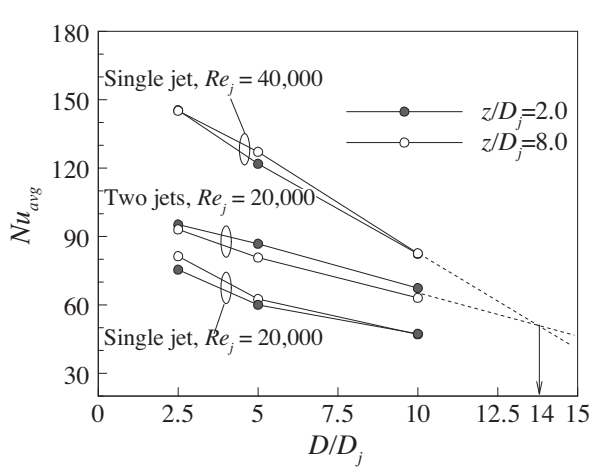

Fig. 15. Comparison of overall heat removal from target cylinders having different relative sizes; $D/Dj = 2.5$, 5.0, and 10.0.

4. Practical implication

Thermo-physically, the laminar to turbulent transition plays an important role in enhancing local heat transfer on a target circular cylinder (larger than the jet diameter) in crossflow if positioned inside the potential core of the jet flow. With a single jet impinging on a cylinder, the laminar to turbulent transition always takes place (Fig. 14(a)). However, with the second counter jet introduced at $\alpha = 180°$, the target cylinder's relative size determines the occurrence of the transition. If it is too small (e.g., $D/D_j = 2.5$); the transition does not take place since there is no enough circumferential space between the stagnation point and the reverse flow region for the flow to undergo the transition (Fig. 14(b)). If the cylinder is large enough e.g., $D/D_j = 5.0$ and 10.0, even with the two-counter jets, the transition can occur as illustrated in Fig. 14(c). In terms of engineering application, the superior cooling by a single jet to two-counter jets for a fixed total flow rate in the present D/D_j ranges is evident. However, assuming the validity of the extrapolated data, the two-counter jets may remove more heat if $D/D_j \geqslant 14.0$ (Fig. 15). The concentrated cooling on the fore side of a target cylinder that determines the overall heat transfer is more effective if a target cylinder is relatively small ($D/D_j < 14.0$). However, the distributed cooling may become more effective if a target cylinder is sufficiently large ($D/D_j \geqslant 14.0$).

5. Conclusions

Details of circumferential heat transfer distribution on a circular cylinder emitting constant heat flux subject to the cooling by either single or two-counter jets in crossflow were experimentally considered. Three target cylinders ($D/D_j = 2.5$, 5.0 and 10.0) positioned at two distinctive impinging distances; $z/D_j = 2.0$ (inside the potential core) and 8.0 (outside the potential core) with the potential core persisting up to $z/D_j = 4.0$ were separately considered. Comparisons were made for a fixed jet Reynolds number and for a fixed total mass flow rate. New findings in the present study are summarized as follows.

(1) Laminar to turbulent transition takes place only if the target cylinder is positioned inside the potential core of jet flow. However, with two-counter jet impingement, the transition requires a certain distance between the stagnation point and the reverse flow region determined by the D/D_j ratio as $T = \pi D/4$.
(2) With two counter-jets, a reverse flow region which elevates local heat transfer is always formed but its effect diminishes as the target cylinder becomes larger.
(3) It is laminar to turbulent transition rather than flow separation on a target cylinder that increases local heat transfer. The contribution of the transition to overall heat transfer becomes localized and eventually minimal as the D/D_j ratio is increased.

Conflict of interest

None declared.

Acknowledgements

This study was supported by the Korea Ministry of Science and Technology via the South Korea–South Africa Research Center Program (Grant No.: 0420-20110129), by the NRF South Africa Incentive Fund for rated researchers, by the National 111 Project of China (Grant No.: B06024) and by the National Basic Research Program of China (Grand No.: 2011CB610305).

References

[1] H. Martin, Heat and mass transfer between impinging gas jets and solid surfaces, Adv. Heat Transfer 13 (1977) 1–60.
[2] J.N.B. Livingood, P. Hrycak, Impingement heat transfer from turbulent air jets to flat plates – a literature survey, NASA, TM X-2778, 1973.
[3] K. Jambunathan, E. Lai, M.A. Moss, B.L. Button, A review of heat-transfer data for single circular jet impingement, Int. J. Heat Fluid Flow 13 (2) (1992) 106–115.
[4] J.W. Gauntner, J.N.B. Livingood, P. Hrycak, Survey of literature on flow characteristics of a single turbulent jet impinging on a flat plate, NASA, TN D-5652 NTIS N70–18963, 1970.
[5] R. Gardon, J.C. Akfirat, The role of turbulence in determining the heat-transfer characteristics of impinging jets, Int. J. Heat Mass Transfer 8 (10) (1965) 1261–1272.
[6] H.M. Hofmann, M. Kind, H. Martin, Measurements on steady state heat transfer and flow structure and new correlations for heat and mass transfer in submerged impinging jets, Int. J. Heat Mass Transfer 50 (19–20) (2007) 3957–3965.
[7] Q.C. Zhang, T.J. Lu, S.Y. He, D.P. He, Control of pore morphology in closed-celled aluminum foams(in Chinese), J. Xi'an Jiaotong Univ. 41 (3) (2007) 255–270.
[8] Y. Zou, D. He, J. Jiang, New type of spherical pore Al alloy foam with low porosity and high strength, Sci. China Ser. B: Chem. 47 (5) (2004) 407–413.
[9] C. Cornaro, A.S. Fleischer, M. Rounds, R.J. Goldstein, Jet impingement cooling of a convex semi-cylindrical surface, Int. J. Therm. Sci. 40 (10) (2001) 890–898.
[10] D.H. Lee, Y.S. Chung, D.S. Kim, Turbulent flow and heat transfer measurements on a curved surface with a fully developed round impinging jet, Int. J. Heat Fluid Flow 18 (1) (1997) 160–169.
[11] E.M. Sparrow, C.A.C. Altemani, A. Chaboki, Jet-impingement heat-transfer for a circular jet impinging in cross-flow on a cylinder, J. Heat Transfer – Trans. ASME 106 (3) (1984) 570–577.
[12] A.A. Tawfek, Heat transfer due to a round jet impinging normal to a circular cylinder, Heat Mass Transfer 35 (4) (1999) 327–333.
[13] X.L. Wang, H.B. Yan, T.J. Lu, S.J. Song, T. Kim, Heat transfer characteristics of an inclined impinging jet on a curved surface in crossflow, J. Heat Transfer 136 (8) (2014) 081702.
[14] X.L. Wang, D. Motala, T.J. Lu, S.J. Song, T. Kim, Heat transfer of a circular impinging jet on a circular cylinder in crossflow, Int. J. Therm. Sci. 78 (2014) 1–8.
[15] D. Singh, B. Premachandran, S. Kohli, Experimental and numerical investigation of jet impingement cooling of a circular cylinder, Int. J. Heat Mass Transfer 60 (2013) 672–688.
[16] K.B. Lim, C.H. Lee, N.W. Sung, S.H. Lee, An experimental study on the characteristics of heat transfer on the turbulent round impingement jet according to the inclined angle of convex surface using the liquid crystal transient method, Exp. Therm. Fluid Sci. 31 (7) (2007) 711–719.
[17] C. Cornaro, A.S. Fleischer, R.J. Goldstein, Flow visualization of a round jet impinging on cylindrical surfaces, Exp. Therm. Fluid Sci. 20 (2) (1999) 66–78.
[18] A.M. Huber, R. Viskanta, Effect of jet-jet spacing on convective heat transfer to confined, impinging arrays of axisymmetric air jets, Int. J. Heat Mass Transfer 37 (18) (1994) 2859–2869.
[19] B.P. Dano, J.A. Liburdy, K. Kanokjaruvijit, Flow characteristics and heat transfer performances of a semi-confined impinging array of jets: effect of nozzle geometry, Int. J. Heat Mass Transfer 48 (3) (2005) 691–701.
[20] D.H. Rhee, P.H. Yoon, H.H. Cho, Local heat/mass transfer and flow characteristics of array impinging jets with effusion holes ejecting spent air, Int. J. Heat Mass Transfer 46 (6) (2003) 1049–1061.
[21] N. Zuckerman, N. Lior, Jet impingement heat transfer: physics, correlations, and numerical modeling, Adv. Heat Transfer 39 (2006) 565–631.
[22] R. Goldstein, J. Timmers, Visualization of heat transfer from arrays of impinging jets, Int. J. Heat Mass Transfer 25 (12) (1982) 1857–1868.
[23] B. Bellhouse, D.L. Schultz, Determination of mean and dynamic skin friction, separation and transition in low-speed flow with a thin-film heated element, J. Fluid Mech. 24 (02) (1966) 379–400.
[24] A. Wietrzak, R.M. Lueptow, Wall shear stress and velocity in a turbulent axisymmetric boundary layer, J. Fluid Mech 259 (1994) 191–218.
[25] Y. Chew, B. Khoo, C. Lim, C. Teo, Dynamic response of a hot-wire anemometer. Part II: A flush-mounted hot-wire and hot-film probes for wall shear stress measurements, Measure. Sci. Technol. 9 (5) (1998) 764.
[26] O. Desgeorges, T. Lee, F. Kafyeke, Multiple hot-film sensor array calibration and skin friction measurement, Exp. Fluids 32 (1) (2002) 37–43.
[27] H.W. Coleman, W.G. Steele, Experimentation, Validation, and Uncertainty Analysis for Engineers, third ed., John Wiley, New Jersey, 2009.
[28] G.N. Abramovich, The Theory of Turbulent Jets, MIT Press, Cambridge, MA, USA, 1963.
[29] D. Reungoat, N. Riviere, J.P. Faure, 3C PIV and PLIF measurement in turbulent mixing – round jet impingement, J Visual – Jpn. 10 (1) (2007) 99–110.
[30] F. Giralt, C.J. Chia, O. Trass, Characterization of impingement region in an axisymmetric turbulent jet, Ind. Eng. Chem. Fund. 16 (1) (1977) 21–28.
[31] E. Esirgemez, J.W. Newby, C. Nott, S.M. Olcmen, V. Otugen, Experimental study of a round jet impinging on a convex cylinder, Measure. Sci. Technol. 18 (7) (2007) 1800–1810.
[32] D.H. Lee, J. Song, M.C. Jo, The effects of nozzle diameter on impinging jet heat transfer and fluid flow, J. Heat Transfer – Trans. ASME 126 (4) (2004) 554–557.
[33] R. Goldstein, M. Franchett, Heat transfer from a flat surface to an oblique impinging jet, J. Heat Transfer – Trans. ASME 110 (1988) 84–90.